



Research article

Magnetic properties and magnetoresistance of hybrid multilayer nanostructures $\{[(\text{Co}_{40}\text{Fe}_{40}\text{B}_{20})_{34}(\text{SiO}_2)_{66}]/[\text{ZnO}]\}_n$

Y.E. Kalinin^a, A.V. Sitnikov^a, V.A. Makagonov^{a,*}, V.A. Foshin^a, M.N. Volochaev^b, I.M. Pripechenkov^c, N.N. Perova^c, E.A. Ganshina^c, V.V. Rylkov^d, A.B. Granovsky^c

^a Voronezh State Technical University, 394006 Voronezh, Russia

^b Kirensky Institute of Physics, 660036 Krasnoyarsk, Russia

^c Faculty of Physics, Lomonosov Moscow State University, 119991 Moscow, Russia

^d National Research Center Kurchatov Institute, 123182 Moscow, Russia



ARTICLE INFO

Keywords:

Hybrid multilayers
Nanostructures
Magnetization
Negative magnetoresistance

ABSTRACT

The structural, electrical, magnetic, magneto-optical properties and magnetoresistance of $\{[(\text{Co}_{40}\text{Fe}_{40}\text{B}_{20})_{34}(\text{SiO}_2)_{66}]/[\text{ZnO}]\}_n$ multilayer structures, where $n = 50$ is the number of bilayers $(\text{Co}_{40}\text{Fe}_{40}\text{B}_{20})_{34}(\text{SiO}_2)_{66}$ nanocomposite and ZnO have been studied. The thicknesses of $(\text{Co}_{40}\text{Fe}_{40}\text{B}_{20})_{34}(\text{SiO}_2)_{66}$ nanocomposite layers as well as ZnO spacers were varied in a wide range. The samples were synthesized by ion-beam sputtering onto glass ceramic substrates. The $(\text{Co}_{40}\text{Fe}_{40}\text{B}_{20})_{34}(\text{SiO}_2)_{66}$ composite have an amorphous structure and the semiconductor ZnO interlayers have a hexagonal crystalline structure with the p63mc symmetry group. The nanocomposite layers containing a ferromagnetic component far from the percolation threshold are in a superparamagnetic state. The presented in the paper data of magnetization, magneto-optical transverse Kerr effect and magnetoresistance indicates that long-range ferromagnetic order does not form down to 77 K both for references ZnO films and studied multilayers with thin and thick ZnO interlayers. An increase in the magneto-optical signal in multilayers compared to references $(\text{Co}_{40}\text{Fe}_{40}\text{B}_{20})_{34}(\text{SiO}_2)_{66}$ composite films has been detected at 1.2 eV. The magnetoresistance of $\{[(\text{Co}_{40}\text{Fe}_{40}\text{B}_{20})_{34}(\text{SiO}_2)_{66}]/[\text{ZnO}]\}_n$ multilayers with thick (>32 nm) ZnO interlayers is lower than in reference $(\text{Co}_{40}\text{Fe}_{40}\text{B}_{20})_{34}(\text{SiO}_2)_{66}$ nanocomposite, while at thin ZnO interlayers magnetoresistance is significantly higher and reaches 12 % at temperatures of 77 K. Possible mechanisms of ferromagnetic and antiferromagnetic ordering, enhancement of the magneto-optical response and magnetoresistance in $\{[(\text{Co}_{40}\text{Fe}_{40}\text{B}_{20})_{34}(\text{SiO}_2)_{66}]/[\text{ZnO}]\}_n$ multilayer nanostructures are discussed.

1. Introduction

Hybrid multilayer structures “magnetic nanocomposite-semiconductor” with ultrathin interlayers, where the magnetic nanocomposite is a system of superparamagnetic particles distributed within dielectric matrix, can manifest not only properties of the constituent layers, but new characteristics also due to possible effects of magnetic proximity and exchange interaction between the layers [1–5]. On the one side, the magnetic proximity effect or diffusion of magnetic ions into the semiconductor can initiate the ferromagnetic state of the semiconductor layer. On the other side, the exchange interaction between ferromagnetic granules of nanocomposite layers via semiconductor layer can induce ferromagnetic ordering within nanocomposite layers, ferromagnetic or antiferromagnetic ordering of the magnetic moments

between the adjacent layers, strengthen or weaken magnetoresistance and other magnetotransport or magneto-optical effects [6–9].

The physical properties of such hybrid systems, where the monolayer thickness is on the order of several nanometers, are greatly determined by the structure and interface phenomena between different phases and can be realized by simple technological approaches by changing the material and thickness of the interlayers. Particular interest in these systems is explained by the possibility of practical use of the giant magnetoresistance effect, which can arise both due to spin-dependent transport phenomena in nanocomposite layers and between layers. At the same time, the technology for manufacturing hybrid multilayers is relatively simpler than in “ferromagnetic metal-transition metal” or “ferromagnetic metal-dielectric” multilayers, because does not require epitaxial growth of films and the use of “clean rooms”, and the presence

* Corresponding author.

E-mail address: vlad_makagonov@mail.ru (V.A. Makagonov).

<https://doi.org/10.1016/j.jmmm.2024.172287>

Received 27 April 2024; Received in revised form 15 June 2024; Accepted 24 June 2024

Available online 25 June 2024

0304-8853/© 2024 Elsevier B.V. All rights reserved, including those for text and data mining, AI training, and similar technologies.

of bridges between the layers is not critical. Hybrid multilayers of a certain composition with ferromagnetic ordering of nanocomposite layers can also be promising for high-frequency applications due to their magnetic softness and high resistivity. It is also possible to create magneto-optical materials with enhanced response.

Preliminary studies of such systems were carried out mainly on the $\text{Co}_{45}\text{Fe}_{45}\text{Zr}_{10}\text{Al}_2\text{O}_3$ and $(\text{Co}_{40}\text{Fe}_{40}\text{B}_{20})_{50}(\text{SiO}_2)_{50}/\text{SiO}_2$ systems [6–9], and with a limited range of parameters. These studies demonstrated the occurrence of ferromagnetic ordering at nanocomposite-semiconductor interfaces at certain thicknesses of the semiconductor layer, when superparamagnetic granules are not in contact with each other inside the nanocomposite layer. The magneto-transport properties of hybrid multilayers have not been studied.

In this work, we study the structural, magnetic, magneto-optical, electrical properties and magnetoresistance of hybrid multilayers $\{[(\text{Co}_{40}\text{Fe}_{40}\text{B}_{20})_{34}(\text{SiO}_2)_{66}]/[\text{ZnO}]\}_n$ (where n is the number of $(\text{Co}_{40}\text{Fe}_{40}\text{B}_{20})_{34}(\text{SiO}_2)_{66}$ nanocomposite and ZnO bilayers) in a wide range of thicknesses of $(\text{Co}_{40}\text{Fe}_{40}\text{B}_{20})_{34}(\text{SiO}_2)_{66}$ nanocomposite and ZnO semiconductor layers. The properties of $(\text{Co}_{40}\text{Fe}_{40}\text{B}_{20})_{34}(\text{SiO}_2)_{66}$ nanocomposites have been well studied, and at selected concentration of $\text{Co}_{40}\text{Fe}_{40}\text{B}_{20}$ ferromagnetic phase with a high degree of spin polarization, the nanocomposite is an ensemble of non-contacting superparamagnetic granules that weakly interact at room temperature. The choice of ZnO as a semiconductor is conditioned to the next facts. Firstly, the presence of ferromagnetic ordering in this material without or with the addition of transition metals (see, for example, [10,11] and references in these works). Secondly, ZnO can be successfully integrated into various hybrid devices, for example with graphene [12]. A detailed review of the properties of ZnO, materials and devices based on it is given in [13]. We observed the strong influence of ZnO spacer thickness on studied properties and found enhanced magnetoresistance and magneto-optical response at certain compositions.

2. Samples and experimental procedure

The preparation of multilayer structures $\{[(\text{Co}_{40}\text{Fe}_{40}\text{B}_{20})_{34}(\text{SiO}_2)_{66}]/[\text{ZnO}]\}_n$ was carried out by ion-beam method with subsequent deposition on a rotating substrate according to the method described in [9,14,15]. To deposit multilayer composite-semiconductor structures, a composite target made of a metal alloy $\text{Co}_{40}\text{Fe}_{40}\text{B}_{20}$ base with thirteen SiO_2 plates uniformly distributed on its surface, as well as a target made of zinc oxide semiconductor, were used (see the scheme of the composite target in [16]). During the deposition process, a V-shaped screen was installed between ZnO target and the substrate, which made it possible to adjust the thickness of the semiconductor interlayer over a wide range. Substrates were fixed on a substrate holder parallel to the target plane along its long side. Then, based on the selected process parameters, two targets were sputtered simultaneously. The multilayer structure had several bilayers, which was determined by a compromise between the duration of deposition and the film thickness to increase the signal of magnetodynamic measurements. As it was previously established if the number of bilayers was more than 10, the magnetic properties of the structures practically did not change. Therefore, we settled on choosing the number of bilayers equal to 50, in such a way that the final formula of the resulting multilayer structures can be written in the form $\{[(\text{Co}_{40}\text{Fe}_{40}\text{B}_{20})_{34}(\text{SiO}_2)_{66}]/[\text{ZnO}]\}_{50}$. A series of reference nanocomposite samples $(\text{Co}_{40}\text{Fe}_{40}\text{B}_{20})_X(\text{SiO}_2)_{100-X}$ (where X is $\text{Co}_{40}\text{Fe}_{40}\text{B}_{20}$ metal phase content in atomic percentage) and ZnO films were also obtained. To obtain $(\text{Co}_{40}\text{Fe}_{40}\text{B}_{20})_X(\text{SiO}_2)_{100-X}$ composites with different contents of the metal phase X in a single technological process, a target with a nonuniform distribution of SiO_2 plates on the surface of $\text{Co}_{40}\text{Fe}_{40}\text{B}_{20}$ base was used. As substrates glass ceramics for measuring electrical, magnetic, magnetoresistive and magneto-optical measurements were used, as well as monocrystalline silicon with the orientation (001) for X-ray measurements.

In order to determine the optimal conditions to deposition of

multilayer structures with interlayers of the order of several nanometers, references $(\text{Co}_{40}\text{Fe}_{40}\text{B}_{20})_{34}(\text{SiO}_2)_{66}$ composite and ZnO films were separately synthesized on substrates, alternately occupying composite and ZnO deposition positions (the substrate holder rotated around the axis of the sputtering chamber). The thickness values of the reference $(\text{Co}_{40}\text{Fe}_{40}\text{B}_{20})_{34}(\text{SiO}_2)_{66}$ composite and ZnO films, measured at several points of the substrate holder by optical interferometry, were divided by the number of substrate holder revolutions, which gave preliminary values of the thicknesses for $(\text{Co}_{40}\text{Fe}_{40}\text{B}_{20})_{34}(\text{SiO}_2)_{66}$ composite and ZnO interlayers, which is expected to obtain in a multilayer structure. The exact thicknesses of the composite and ZnO interlayers in the multilayer structure were determined by X-ray diffraction in the region of small Bragg angles and transmission electron microscopy.

The chemical composition of the films was carried out using an Oxford INCA Energy 250 energy-dispersive X-ray attachment on a JEOL JSM-6380 LV scanning electron microscope. The structure was studied by X-ray diffraction methods on a Bruker D2 Phaser diffractometer ($\lambda_{\text{CuK}\alpha 1} = 1.54 \text{ \AA}$) using DIFFRAC.EVA 3.0 software with the ICDD PDF Release 2012 database. Transmission electron micrograph (TEM) of a transverse section and electron diffraction images were obtained at Hitachi HT7700 microscope at an accelerating voltage of 100 kV (W source). Transverse sections with a thickness of approximately 40–50 nm were prepared using a single-beam focused ion beam system (FIB, Hitachi FB2100). To protect the films from destruction during the preparation of the section, the sample was precoated with a protective film of amorphous germanium.

The dependences of the electrical resistivity were measured using a two-probe method at direct current using a universal digital multimeter B7-78/1. To study the influence of an external magnetic field on the electrical conductivity of the studied samples, the latter were placed between the poles of an electromagnet so that the magnetic field was directed in the plane of the sample perpendicular to its plane.

Magnetic properties were studied with a LakeShore (USA) vibration sample magnetometer, model 7407 in fields up to 16 kOe. We also used a MPMS XL7 SQUID (Quantum Design) magnetometer to study magnetic properties of ZnO at 2 K.

Magneto-optical (MO) studies were carried out in the geometry of the transverse Kerr effect (TKE) [17,18] at $T = 20\text{--}300 \text{ K}$ in the spectral range of 0.5–4.0 eV in a magnetic field up to 3.0 kOe. p-polarized light was used at an incidence angle of 69.5° . For each sample, the spectral dependence in the maximum magnetic field, temperature and field dependence of the MO signal were measured for the selected wavelengths. The measurements were performed using a dynamic method, in which the TKE parameter is the relative change in the intensity of the reflected light when the sample is magnetized by an alternating magnetic field with a frequency of 40 Hz.

3. Experimental results and discussion

3.1. Structure of the studied films

Fig. 1 shows X-ray diffraction patterns of $\{[(\text{Co}_{40}\text{Fe}_{40}\text{B}_{20})_{34}(\text{SiO}_2)_{66}]/[\text{ZnO}]\}_{50}$ multilayer structures with different thickness of ZnO interlayers, $(\text{Co}_{40}\text{Fe}_{40}\text{B}_{20})_{34}(\text{SiO}_2)_{66}$ nanocomposite and ZnO films obtained by deposition on a rotating substrate. Analysis of the presented X-ray diffraction patterns showed that composite interlayers of the synthesized films, as well as reference composite $(\text{Co}_{40}\text{Fe}_{40}\text{B}_{20})_{34}(\text{SiO}_2)_{66}$, have an amorphous structure and ZnO interlayers have a hexagonal crystalline structure with the symmetry group P63mc (Fig. 1a) [19]. It should be noted, that the diffraction pattern of reference ZnO film characterized by the presence of a narrow diffraction maximum at $2\theta \approx 34^\circ$ (Fig. 1a), which can be classified as (0001) planes of hexagonal ZnO cell. An increase in the thickness of ZnO interlayers in the multilayer structure $\{[(\text{Co}_{40}\text{Fe}_{40}\text{B}_{20})_{34}(\text{SiO}_2)_{66}]/[\text{ZnO}]\}_{50}$ leads to an increase in the diffraction maximum, however, its width is significantly greater than that observed for pure ZnO. The presence of only one reflection

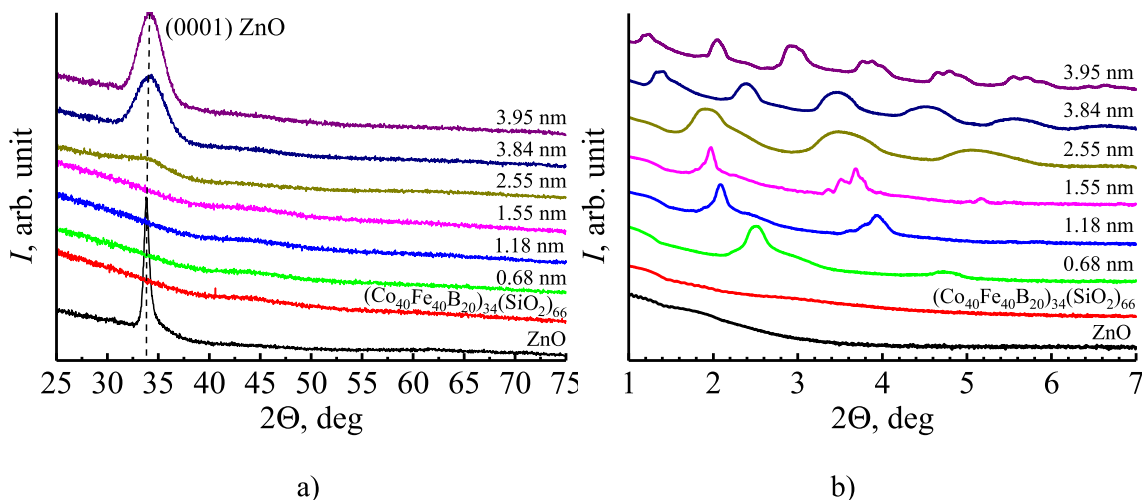


Fig. 1. X-ray diffraction patterns of ZnO films, composite $(\text{Co}_{40}\text{Fe}_{40}\text{B}_{20})_{34}(\text{SiO}_2)_{66}$ and multilayer structures $\{[(\text{Co}_{40}\text{Fe}_{40}\text{B}_{20})_{34}(\text{SiO}_2)_{66}]/[\text{ZnO}]\}_{50}$ with different ZnO interlayer thicknesses, measured at average (a) and small (b) Bragg angles.

maximum (0001) is due to the strong texture. In this case, at small thicknesses of the interlayers, the ZnO crystal structure apparently does not form.

X-ray diffraction at small Bragg angle ($2\theta = 1\text{--}7^\circ$) revealed the presence of diffraction maxima in all of the studied multilayers $\{[(\text{Co}_{40}\text{Fe}_{40}\text{B}_{20})_{34}(\text{SiO}_2)_{66}]/[\text{ZnO}]\}_{50}$ (Fig. 1b), which can be interpreted as the presence of a multilayer structure of the films with different interlayers thicknesses. It should be noted, that for references $(\text{Co}_{40}\text{Fe}_{40}\text{B}_{20})_{34}(\text{SiO}_2)_{66}$ nanocomposite and ZnO films, obtained by deposition on a rotating substrate, there is no maxima at mentioned range.

Diffraction studies using transmission electron microscopy (TEM) confirmed the amorphous structure of the constituent layers of the film at thin ZnO interlayer thickness (inset to Fig. 2), and micrographs of the cross section of the $\{[(\text{Co}_{40}\text{Fe}_{40}\text{B}_{20})_{34}(\text{SiO}_2)_{66}]/[\text{ZnO}]\}_{50}$ system – the formation of composite interlayers $(\text{Co}_{40}\text{Fe}_{40}\text{B}_{20})_{34}(\text{SiO}_2)_{66}$ and multilayer structure (Fig. 2), while the thickness of the interlayers in the studied sample $(\text{Co}_{40}\text{Fe}_{40}\text{B}_{20})_{34}(\text{SiO}_2)_{66}$ was equal to 1.1 nm, and 1.2 nm for ZnO.

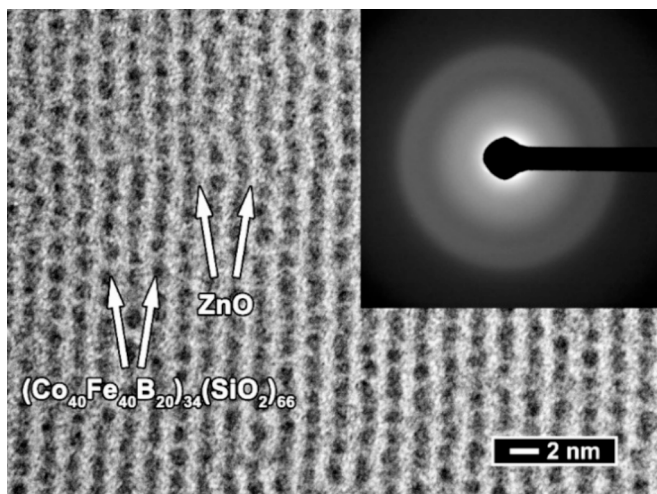


Fig. 2. TEM microimage of the cross section of the multilayer structure $\{[(\text{Co}_{40}\text{Fe}_{40}\text{B}_{20})_{34}(\text{SiO}_2)_{66}]/[\text{ZnO}]\}_{50}$ (the inset shows the diffraction pattern of the film under study).

3.2. Electrical properties of films with a multilayer structure $\{[(\text{Co}_{40}\text{Fe}_{40}\text{B}_{20})_{34}(\text{SiO}_2)_{66}]/[\text{ZnO}]\}_{50}$

Fig. 3a shows the dependences of the electrical resistivity of $(\text{Co}_{40}\text{Fe}_{40}\text{B}_{20})_x(\text{SiO}_2)_{100-x}$ nanocomposites on concentration of the metal phase $\text{Co}_{40}\text{Fe}_{40}\text{B}_{20}$ (designated as X) measured at room temperature. In the case of a composite target with an uneven arrangement of silicon plates on metal $\text{Co}_{40}\text{Fe}_{40}\text{B}_{20}$ plate sputter, the concentration of the metal phase X changes from 25 to 64 at. %, which leads to a non-linear decrease in the electrical resistance of the $(\text{Co}_{40}\text{Fe}_{40}\text{B}_{20})_x(\text{SiO}_2)_{100-x}$ system by approximately 5 orders of magnitude (black curve in Fig. 3a). The obtained dependence is typical for many heterogeneous systems metal–insulator, and a significant decrease in the electrical resistivity of composites with increasing concentration of a metal phase is associated with the transition from a non-metallic type of conductivity to a metallic one. A characteristic feature of this dependence is the deviation from monotonic behavior for compositions located near the percolation threshold, which is especially noticeable after heat treatment in vacuum atmosphere at $T = 400^\circ\text{C}$, 30 min, which does not lead to crystallization of amorphous phases (red curve in Fig. 3a). In this case, heat treatment of composites leads to an increase in the electrical resistance of composites located before and to its decrease beyond the percolation threshold (shown by arrows in Fig. 3a). Thus, the electrical resistance of the selected for obtaining multilayer structures composite layer with the composition of $(\text{Co}_{40}\text{Fe}_{40}\text{B}_{20})_{34}(\text{SiO}_2)_{66}$, depending on the relaxed state of the amorphous phase and deposition conditions, should be greater than 1–10 Ohm·m and the composite itself should be classified as pre-percolation one.

The presence of ZnO interlayers, which has a 3–4 orders of magnitude lower electrical resistivity value, according to our data amounting to $\sim 2.7 \cdot 10^{-4}$ Ohm·m should lead to a decrease in ρ of $\{[(\text{Co}_{40}\text{Fe}_{40}\text{B}_{20})_{34}(\text{SiO}_2)_{66}]/[\text{ZnO}]\}_{50}$ multilayer structures, which is what is happening. Experimental studies of electrical resistivity of the synthesized multilayer structures $\{[(\text{Co}_{40}\text{Fe}_{40}\text{B}_{20})_{34}(\text{SiO}_2)_{66}]/[\text{ZnO}]\}_{50}$ depending on the thickness of ZnO semiconductor interlayers are presented at Fig. 3b. The electrical resistivity ρ of $\{[(\text{Co}_{40}\text{Fe}_{40}\text{B}_{20})_{34}(\text{SiO}_2)_{66}]/[\text{ZnO}]\}_{50}$ multilayers changes slightly with the thickness of the interlayer up to $h_{\text{ZnO}} \sim 1.2$ nm, and then decreases by approximately three orders of magnitude at $h_{\text{ZnO}} = 4$ nm (Fig. 3b). It should be noted that a similar pattern was observed for multilayer structures obtained from $(\text{Co}_{40}\text{Fe}_{40}\text{B}_{20})_{34}(\text{SiO}_2)_{66}$ composite with interlayers of Si, C, Cu, and Bi_2Te_3 [9]. It was found that if the interlayer had a composition with $\rho \ll 0.005$ Ohm + m, the value of $\rho(h)$ changed by more than three orders of magnitude. In the studied $\{[(\text{Co}_{40}\text{Fe}_{40}\text{B}_{20})_{34}(\text{SiO}_2)_{66}]/$

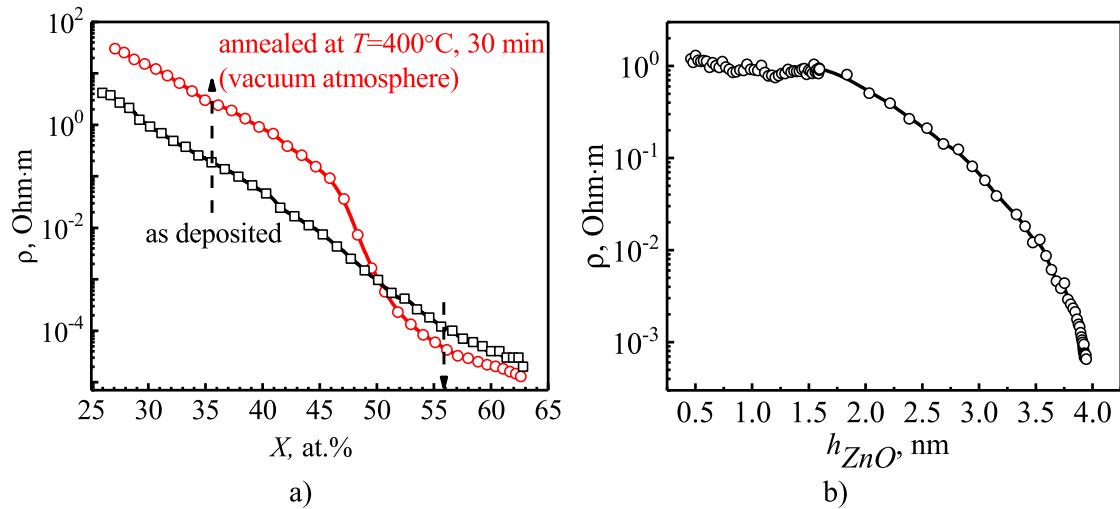


Fig. 3. Electrical resistivity of $(\text{Co}_{40}\text{Fe}_{40}\text{B}_{20})_X(\text{SiO}_2)_{1-X}$ composite films as a function of metal phase content X (a) and resistivity of multilayer structures $\{[(\text{Co}_{40}\text{Fe}_{40}\text{B}_{20})_{34}(\text{SiO}_2)_{66}]/[\text{ZnO}]]_{50}$ depending on the thickness of the ZnO interlayers h_{ZnO} (b).

$[\text{ZnO}]_{50}$ systems, ZnO interlayers also has a lower value of electrical resistivity compared to the electrical resistivity of composite films up to the percolation threshold (Fig. 3a), which also leads to a change in ρ by more than three orders of magnitude with a change in the thickness of ZnO spacers (Fig. 3b).

To explain the observed patterns, let us consider the sequence of growth of the semiconductor layer during the deposition process. The multilayer structure $\{[(\text{Co}_{40}\text{Fe}_{40}\text{B}_{20})_{34}(\text{SiO}_2)_{66}]/[\text{ZnO}]]_{50}$ is a complex heterophase system, one of the main parameters of which is the thickness of the semiconductor layer (h_{ZnO}). At thicknesses of the zinc oxide layer less than ~ 1.2 nm the semiconductor phase has an island structure and is concentrated mainly on metal granules (due to the principle of minimizing the internal energy of the growing film in the process of self-organization) (Fig. 4a). The formed morphology does not significantly affect the processes of electrical transfer in composite $(\text{Co}_{40}\text{Fe}_{40}\text{B}_{20})_{34}(\text{SiO}_2)_{66}$ layers. Increasing ZnO interlayer thicknesses at range of 0.5 to 2 nm results to a lower-resistance conduction channels are formed. At small thicknesses of ZnO interlayers the processes of electrical transfer “metal granule – semiconductor – dielectric – metal granule” can predominate (Fig. 4b), which is observed in the synthesized films (Fig. 3b) at $h_{\text{ZnO}} < 1.5$ nm. As h_{ZnO} increases, the contribution to the conductivity of the “metal granule–semiconductor–metal granule transitions” will increase, and at a thickness of ZnO interlayers more than 2 nm, the electrical resistance is completely determined by these conducting channels of ZnO (Fig. 4c). Some contradiction in the estimates of the island layer thickness of ZnO film from the results of electrical resistance and studies of morphology using transmission electron microscopy, where at thicknesses of ~ 1.2 nm continuous ZnO interlayers are formed, can be associated with applying of different substrate types for electron microscopy (monocrystalline Si (001)) and for electrical properties measuring (glass ceramic substrates with greater roughness were used).

3.3. Magnetic properties

As it was noted above, $(\text{Co}_{40}\text{Fe}_{40}\text{B}_{20})_{34}(\text{SiO}_2)_{66}$ composites represent an ensemble of non-contacting superparamagnetic granules that weakly interact at room temperature [20]. The presence of ZnO semiconductor interlayers, which is not ferromagnetic, between the initially superparamagnetic nanocomposite layers changes the magnetization curves.

Measurements of field dependences of magnetization $m(H)$ on a VSM magnetometer of reference ZnO films both at room temperature and 77 K did not reveal any signs of ferromagnetic ordering; the $m(H)$ curves are strictly linear. Additional studies carried out on a MPMS XL7 SQUID

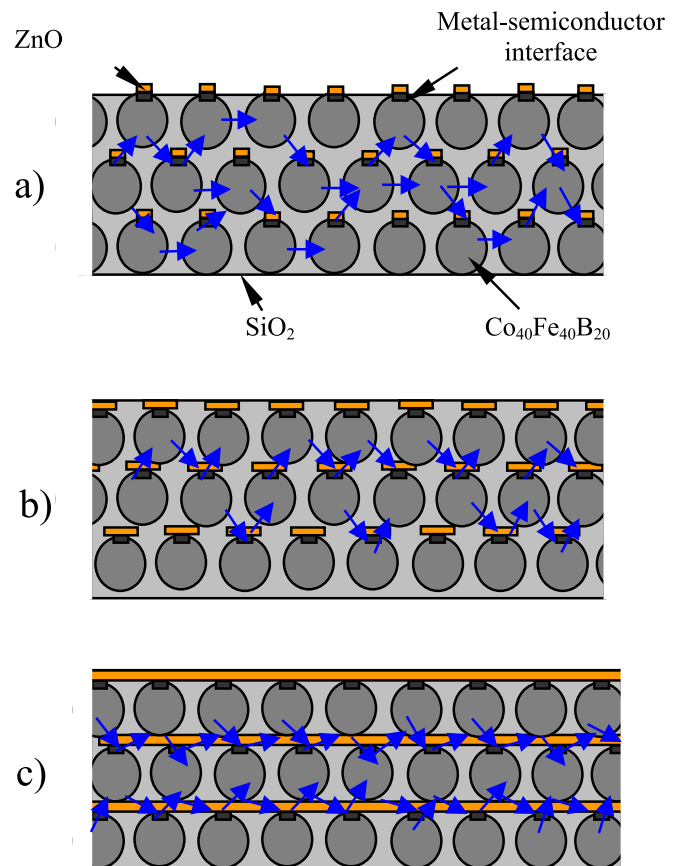


Fig. 4. Model representation of possible current paths (blue arrows) in a multilayer structure $\{[(\text{Co}_{40}\text{Fe}_{40}\text{B}_{20})_{34}(\text{SiO}_2)_{66}]/[\text{ZnO}]]_{50}$ depending on the thickness of ZnO: a – formation of islands of the ZnO semiconductor phase; b – growth of ZnO islands; c – formation of a continuous layer of ZnO. (For interpretation of the references to colour in this figure legend, the reader is referred to the web version of this article.)

(Quantum Design) magnetometer at 2 K also did not reveal the presence of hysteresis loops. The equatorial MO Kerr effect, which is proportional to the in-plane component of magnetization, was not detected up to 20 K, which confirms the absence of long-range magnetic order. Ferromagnetism of ZnO is usually associated with defects at grain boundaries

(see [21,22]) and it is believed that defect-induced magnetism is enhanced by the addition of transition metals to ZnO. In our case, we do not observe defect-induced magnetism, which can be due to the insufficient concentration of defects formed as a result during ion-beam deposition of the films.

As example Fig. 5 shows the magnetization curves of two types of multilayers: with a thin ZnO interlayer thickness $h_{\text{ZnO}} = 0.46$ nm (Fig. 5a) and a thick one – $h_{\text{ZnO}} = 3.94$ nm (Fig. 5b), measured using a VSM magnetometer. Both VSM and Kerr magnetometry did not reveal ferromagnetic ordering for all studied samples, since no hysteresis loops were observed either at room or lower temperatures (up to 100 K) with an accuracy of measuring the coercive force of up to 0.1 Oe. Ferromagnetism of the studied multilayers could arise for three reasons: (i) ferromagnetism of ZnO interlayers upon penetration of Co ions into these layers during deposition or after deposition due to diffusion. The presence of such magnetic ions in the interlayers between granules has been demonstrated for some nanocomposites [23]; (ii) ferromagnetic exchange between neighboring granules of nanocomposite layers through a thin ZnO layer; (iii) ferromagnetic exchange in the interface layer of magnetic granules through the surface layer of ZnO and an increase in the blocking temperature of $\text{Co}_{40}\text{Fe}_{40}\text{B}_{20}$ nanogranules in the interface layer due to a change in the magnetic anisotropy constant.

The first mechanism does not work due to the low concentration of transition metal ions incorporated into ZnO. The second and third mechanisms apparently does not work in our case even for ultrathin ZnO thicknesses (about 1 nm), since superexchange interaction – exchange through oxygen ions of the ZnO interlayer (Fe-O-Fe type) or vacancies usually leads to antiferromagnetic ordering [24], the conductivity of ZnO is low to realizing of indirect exchange through conduction electrons of the RKKY type, and the magnetic anisotropy constant of nanograins weakly depends on the surroundings. These mechanisms can be realized when the composition of the nanocomposite layer is in close proximity to the threshold for the formation of long-range magnetic order and/or at a higher conductivity of the semiconductor layer, as was observed in [9].

In order to clarify the nature of the interaction between the nanocomposite layers, we also measured the magnetic permeability of $\{[(\text{Co}_{40}\text{Fe}_{40}\text{B}_{20})_{34}(\text{SiO}_2)_{66}]/[\text{ZnO}]\}_{50}$ multilayer samples at a frequency of 50 MHz at room temperature using the resonance technique described in [9]. The real part of the magnetic permeability of

$\{[(\text{Co}_{40}\text{Fe}_{40}\text{B}_{20})_{34}(\text{SiO}_2)_{66}]/[\text{ZnO}]\}_{50}$ multilayers with thin ZnO interlayers was close to unity, which means the absence of ferromagnetic-type interaction, which does not exclude antiferromagnetic-type interaction, and as noted above may be a consequence of superexchange through oxygen vacancies in thin ZnO layers. Indirect confirmation of antiferromagnetic interaction in this case is the observed increase in magnetoresistance (see paragraph 2.5 below) with thin ZnO layers. In the case of thick ZnO interlayers (>3 nm), as it taking place in early works [6–9], with sufficiently conductive interlayers, high values of magnetic permeability (~ 10) has been observed. This result may be associated with ferromagnetic interaction between layers if the interaction in a multilayer structure between initially non-interacting superparamagnetic granules leads to a correlated orientation of magnetic moments, similar to the formation of a superferromagnetic state [25–27], characterized by an extremely low coercivity and high magnetic permeability [26]. The considerations expressed are exclusively qualitative in nature and require further experimental and theoretical studies.

3.4. Magneto-optical spectra

Examples of MO spectra for $(\text{Co}_{40}\text{Fe}_{40}\text{B}_{20})_{34}(\text{SiO}_2)_{66}$ reference composite and $\{[(\text{Co}_{40}\text{Fe}_{40}\text{B}_{20})_{34}(\text{SiO}_2)_{66}]/[\text{ZnO}]\}_{50}$ multilayers with different ZnO thicknesses are shown at Fig. 6. Since there is no MO response of reference ZnO films, one can expect that the MO spectra of such hybrid systems as multilayers are entirely determined by $(\text{Co}_{40}\text{Fe}_{40}\text{B}_{20})_{34}(\text{SiO}_2)_{66}$ nanocomposite layers. However, this is not the case (Fig. 6). Distinctive peculiarities of the presented data are, firstly, the presence of additional features in relation to $(\text{Co}_{40}\text{Fe}_{40}\text{B}_{20})_{34}(\text{SiO}_2)_{66}$ reference nanocomposites (Fig. 6a, blue and green curves), and secondly, a large signal magnitude for certain compositions. In particular, in multilayers with a ZnO interlayer 2.2 nm thick, an additional negative peak appears at 1.25 eV and TKE reaches high values at 50 K (Fig. 6b).

We exclude the influence of interference effects, since the depth of formation of the MO signal is about 50–100 nm, which is comparable to the total thickness of the samples, and the layers are quite thin. Since TKE is determined not only by MO, but optical parameters also [17,18], the change in the dielectric constant of ZnO in the vicinity of the plasma frequency can be responsible for the observed effect of TKE enhancement.

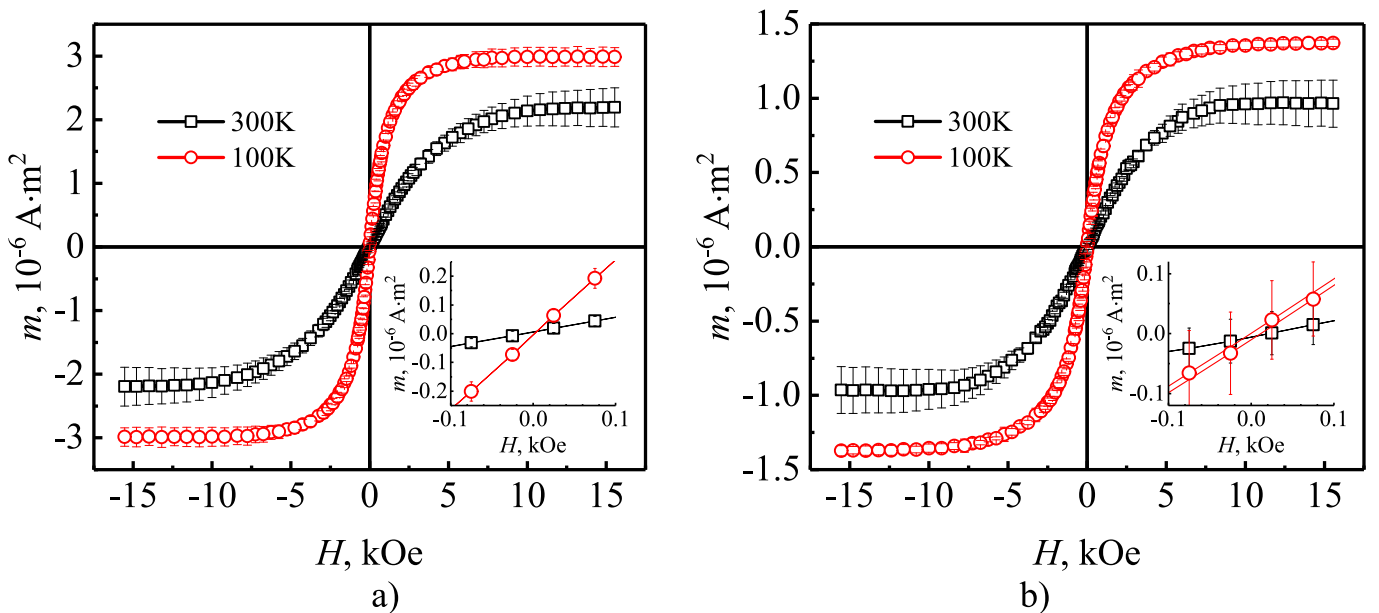


Fig. 5. Magnetization curves of $\{[(\text{Co}_{40}\text{Fe}_{40}\text{B}_{20})_{34}(\text{SiO}_2)_{66}]/[\text{ZnO}]\}_{50}$ multilayers with thin ($h_{\text{ZnO}} = 0.46$ nm) (a) and thick ($h_{\text{ZnO}} = 3.94$ nm) (b) ZnO interlayers, measured using a vibration magnetometer.

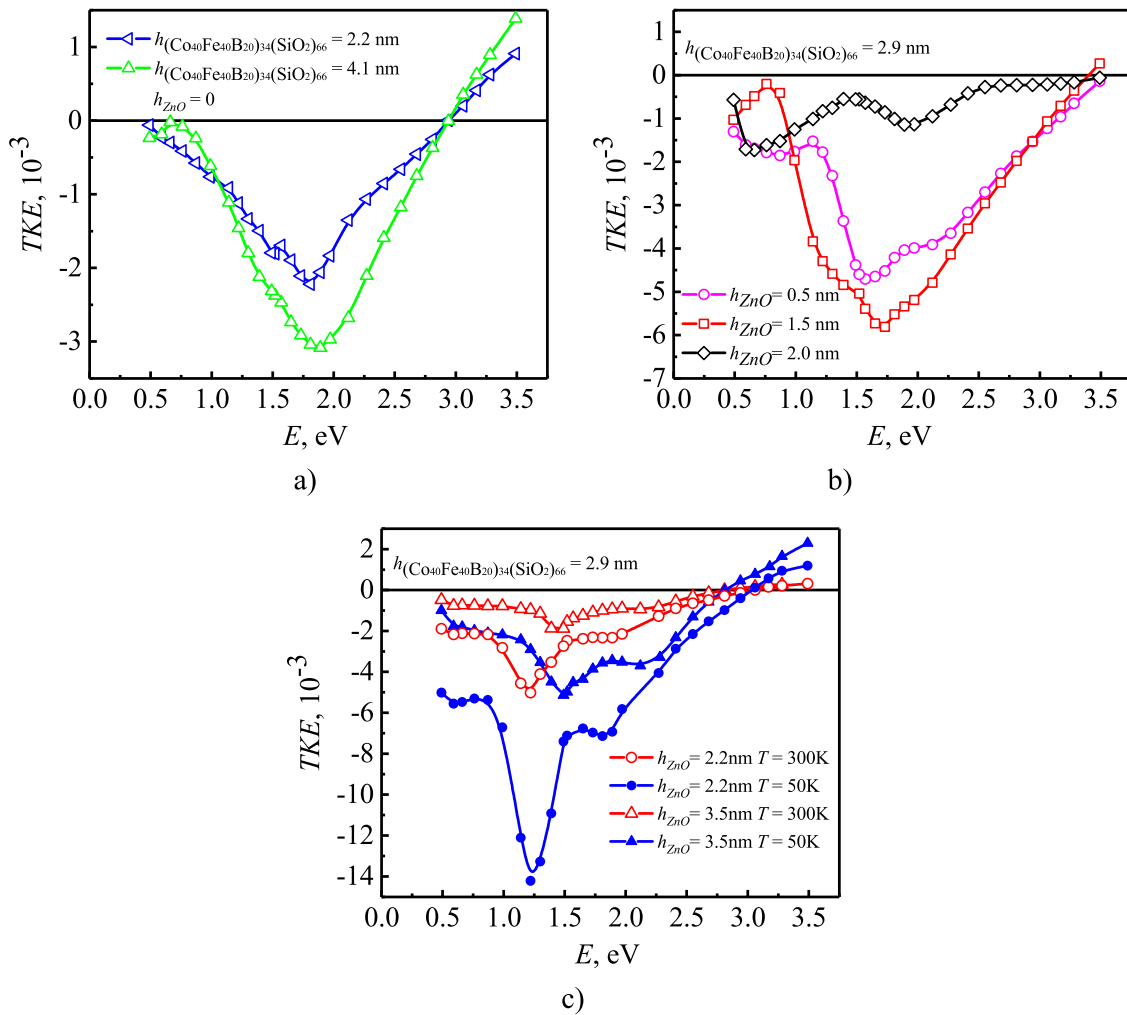


Fig. 6. TKE spectra of $(\text{Co}_{40}\text{Fe}_{40}\text{B}_{20})_{34}(\text{SiO}_2)_{66}$ reference composite film (a) and $\{[(\text{Co}_{40}\text{Fe}_{40}\text{B}_{20})_{34}(\text{SiO}_2)_{66}]/[\text{ZnO}]\}_{50}$ multilayers with different ZnO interlayer thicknesses at room temperature (b) and multilayers with ZnO interlayer thickness of 2.2 nm (circles) and 3.4 nm (triangles) at $T = 50$ K (blue curves) and $T = 300$ K (red curves). Layers thicknesses h of ZnO and nanocomposite are indicated in the corresponding figures. (For interpretation of the references to colour in this figure legend, the reader is referred to the web version of this article.)

The strong non-monotonic dependence of the MO signal on the ZnO interlayer thickness is due to the fact that the MO signal in hybrid multilayers is formed due to the competition of contributions from nanocomposite layers, ZnO interlayers and interfaces. The situation is complicated, firstly, by the fact that the MO signal of thin nanocomposite films also depends on their thickness (green and blue curves in Fig. 6a), since with a change in nanocomposite thickness the size of the granules also changes [17,18], and secondly, it is impossible to exclude the formation of ZnO:Co clusters, which, according to [28], can determine an additional TKE response. At small ZnO interlayer thicknesses of 0.5 nm (Fig. 6b, purple curve), the role of interfaces increases and to an even greater extent at 1.5 nm (red curve), and therefore a sharp increase in the MO signal is observed compared to samples without interlayers. As the thickness of the ZnO interlayer increases, the role of interfaces decreases and the MO signal also decreases and becomes even smaller than in the reference composite (Fig. 6b, black curve).

As the MO temperature decreases, the signal increases, but its spectral profile does not change (Fig. 6c), which confirms the absence of ferromagnetic ordering in the studied samples down to 50 K.

3.5. Magnetoresistance of $\{[(\text{Co}_{40}\text{Fe}_{40}\text{B}_{20})_{34}(\text{SiO}_2)_{66}]/[\text{ZnO}]\}_{50}$ multilayer films

Magnetoresistance (MR) of studied samples was calculated using the standard formula

$$\text{MR} = \{[R(H) - R(0)]/R(0)\} \cdot 100\%, \quad (1)$$

where $R(H)$ is the electrical resistance in any fixed field, $R(0)$ is the electrical resistance in zero magnetic field. In all studied samples, $\{[(\text{Co}_{40}\text{Fe}_{40}\text{B}_{20})_{34}(\text{SiO}_2)_{66}]/[\text{ZnO}]\}_{50}$ multilayers and $(\text{Co}_{40}\text{Fe}_{40}\text{B}_{20})_x(\text{SiO}_2)_{100-x}$ reference nanocomposites the MR is negative (Fig. 7a) and is characterized by a tendency to saturation in strong fields at low temperatures (Fig. 7b), which indicates a spin-dependent tunneling mechanism. An unexpected result is the enhancement of MR in some multilayer systems compared to $(\text{Co}_{40}\text{Fe}_{40}\text{B}_{20})_{34}(\text{SiO}_2)_{66}$ reference nanocomposite with the composition used at obtaining multilayers and the dependence of MR on the thickness of ZnO interlayers. An explanation of these features, which appear at both room and low temperatures, is given below. It is worth noting that the MR in some multilayers is positive and does not saturate [29,30], but in our case MR is negative for all samples.

According to the Inoue-Maekawa theory [31], spin-dependent tunneling in nanocomposites is described by the formula

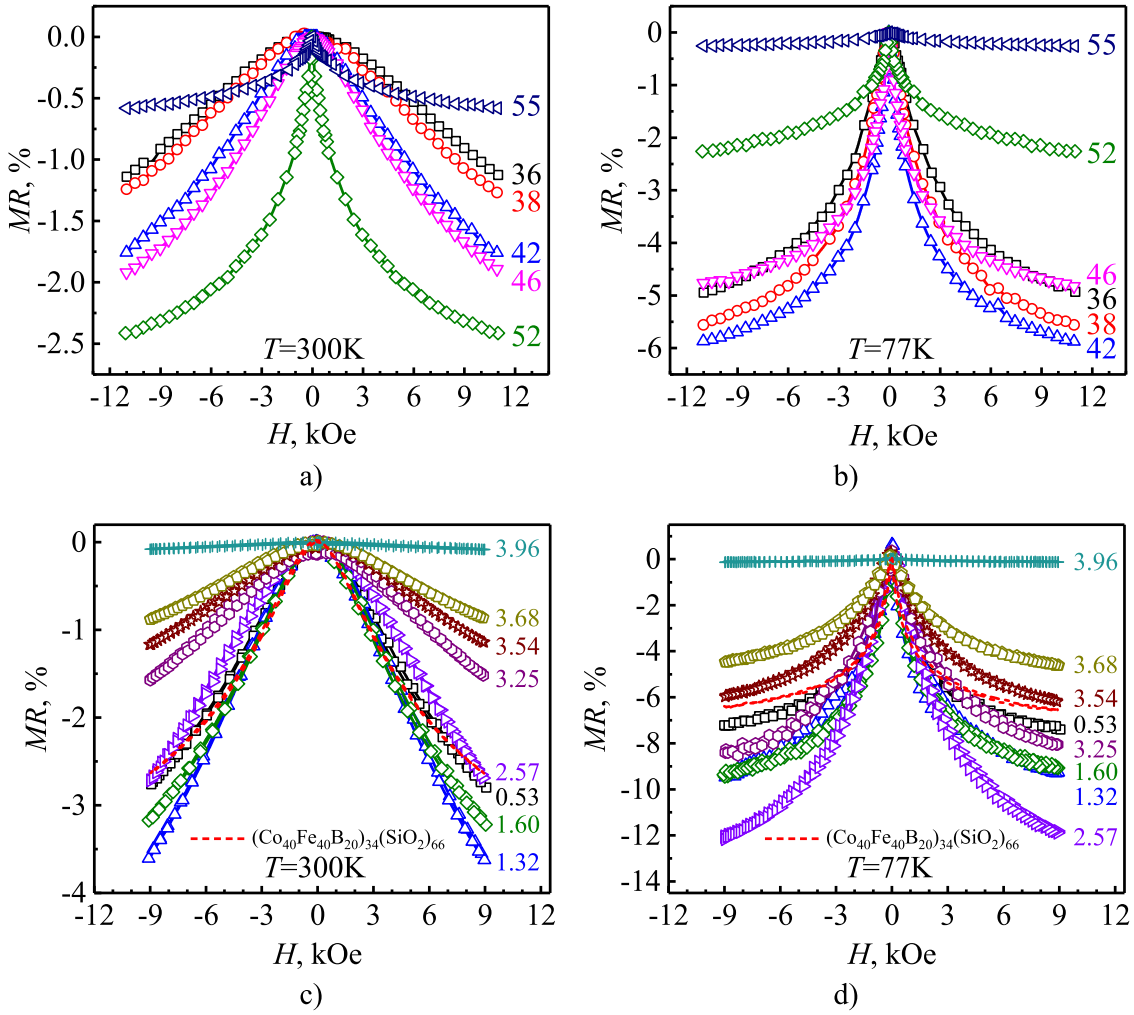


Fig. 7. Magnetic field dependences of magnetoresistance of the composites $(\text{Co}_{40}\text{Fe}_{40}\text{B}_{20})_x(\text{SiO}_2)_{100-x}$ (a, b) (the X values are indicated close to the curves), as well as multilayer structures $\{[(\text{Co}_{40}\text{Fe}_{40}\text{B}_{20})_{34}(\text{SiO}_2)_{66}]/[\text{ZnO}]\}_{50}$ with different ZnO interlayer thicknesses (are indicated close to the curves) (c, d) at room temperature (a, c) and 77 K (b, d).

$$MR = -P^2 \left(\frac{M}{M_S} \right)^2 \quad (2)$$

That is, MR is proportional to the square of the relative magnetization (M and M_S magnetization in a fixed field and saturation magnetization, respectively) and the spin polarization P of the granules. The Inoue-Maekawa theory is based on the concepts developed in [32,33] and is valid only in the close vicinity of the percolation threshold. In particular, the expression does not depend on the concentration of metal phase of a nanocomposite, although it is well known that the MR decreases when the concentration of the ferromagnetic component becomes significantly less than or greater than the percolation threshold. The effect of the ferromagnetic phase content on the MR of $(\text{Co}_{40}\text{Fe}_{40}\text{B}_{20})_x(\text{SiO}_2)_{100-x}$ reference nanocomposites is illustrated at Fig. 7a and b. Far from the percolation transition, the Inoue-Maekawa theory does not work and usually experimental data for pre-percolation compositions are interpreted within the framework of the spin-dependent tunneling model through chains of granules or ions between granules [34–36], which strongly depends on the ferromagnetic metal concentration, that is, on the average distance between granules. In our case, when ZnO layer is thin (see Fig. 4), the distance between $\text{Co}_{40}\text{Fe}_{40}\text{B}_{20}$ granules of neighboring nanocomposite layers becomes smaller than within the nanocomposite layer, and the resistance of the structure decreases due to the lower resistivity of ZnO, which leads to an increase in MR, reaching high values (up to 12 %) (Fig. 7c and d). Fig. 8 summarizes the data of Fig. 7c

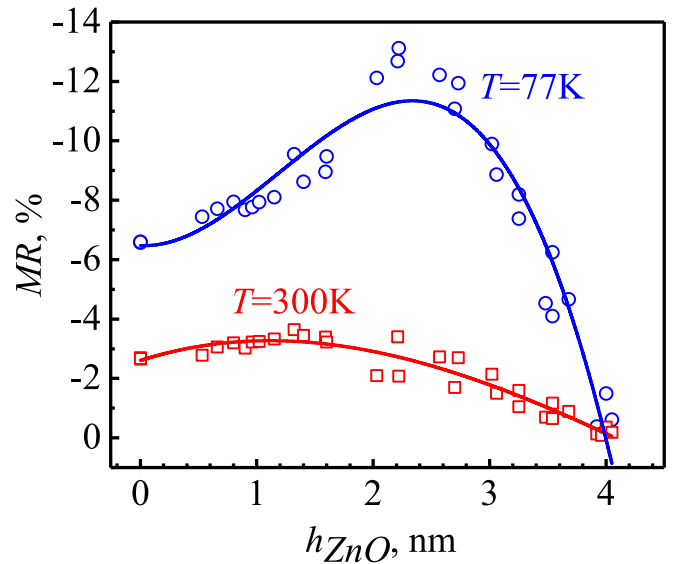


Fig. 8. Magnetoresistance of $\{[(\text{Co}_{40}\text{Fe}_{40}\text{B}_{20})_{34}(\text{SiO}_2)_{66}]/[\text{ZnO}]\}_{50}$ multilayer films as function of ZnO semiconductor interlayers thickness, measured at room temperature $T = 300$ K and at $T = 77$ K.

and d regarding the dependence of MR on ZnO thickness.

It cannot be ruled out that neighboring granules interact antiferromagnetically through a thin ZnO interlayer, thus enhancing the MR due to the formation of an antiparallel orientation of the magnetic moments of the granules in the absence of a magnetic field, which is more favorable for the spin-dependent tunnel-type MR. At thick ZnO interlayers (>3 nm), on the contrary, the MR becomes smaller than in the nanocomposite. This is explained by the fact that the percolation threshold in the nanocomposite layers shifts to the region of the dielectric phase during the transition from a three-dimensional system to a two-dimensional one at the same chemical and phase composition.

4. Conclusions

A comprehensive study of the structural, electrical, magnetic, magneto-optical properties and magnetoresistance of $\{[(\text{Co}_{40}\text{Fe}_{40}\text{B}_{20})_{34}(\text{SiO}_2)_{66}]/[\text{ZnO}]\}_{50}$ multilayer systems showed the dependence of these properties on the thickness of ZnO semiconductor interlayers. We didn't have detect defect-induced magnetism down to 2 K in reference ZnO films, obtained at the same conditions as it was used for $\{[(\text{Co}_{40}\text{Fe}_{40}\text{B}_{20})_{34}(\text{SiO}_2)_{66}]/[\text{ZnO}]\}_{50}$ multilayers. The manifestation of ferromagnetic behavior in $\{[(\text{Co}_{40}\text{Fe}_{40}\text{B}_{20})_{34}(\text{SiO}_2)_{66}]/[\text{ZnO}]\}_{50}$ multilayers due to the effect of magnetic proximity or due to the penetration of transition metal ions in ZnO interlayers during the deposition process was not found also down to 77 K. The main practically important result of the work is the discovery of the enhanced magneto-optical Kerr effect and magnetoresistance. The enhancement of the Kerr effect occurs due to an increase in the electric field accompanying plasma oscillations in ZnO. The magnetoresistance of $\{[(\text{Co}_{40}\text{Fe}_{40}\text{B}_{20})_{34}(\text{SiO}_2)_{66}]/[\text{ZnO}]\}_{50}$ multilayers in a field of 10 kOe at 300 K reaches 4 % at room temperature and 12 % at 77 K, which is twice more than the maximum value obtained for $(\text{Co}_{40}\text{Fe}_{40}\text{B}_{20})_x(\text{SiO}_2)_{100-x}$ reference nanocomposites (see curves at $X = 42$ at.% on Fig. 7a and b).

CRedit authorship contribution statement

Y.E. Kalinin: Writing – original draft, Supervision, Project administration, Conceptualization. **A.V. Sitnikov:** Writing – original draft, Supervision, Resources, Methodology, Formal analysis. **V.A. Makagonov:** Writing – review & editing, Writing – original draft, Visualization, Supervision, Data curation. **V.A. Foshin:** Writing – review & editing, Visualization, Validation, Supervision, Investigation. **M.N. Volochaev:** Writing – review & editing, Methodology, Investigation. **I.M. Pripechenkov:** Visualization, Methodology, Investigation, Data curation. **N.N. Perova:** Writing – original draft, Visualization, Methodology, Investigation, Data curation. **E.A. Ganshina:** Writing – review & editing, Writing – original draft, Supervision, Conceptualization. **V.V. Rylkov:** Writing – original draft, Validation, Conceptualization. **A.B. Granovsky:** Writing – review & editing, Writing – original draft, Supervision, Formal analysis, Conceptualization.

Declaration of competing interest

The authors declare the following financial interests/personal relationships which may be considered as potential competing interests: Y. E. Kalinin reports financial support was provided by The work was carried out with the support of the Ministry of Science and Higher Education of the Russian Federation within the framework of a state assignment (project No. FZGM-2023-0006). A.V. Sitnikov reports financial support was provided by The work was carried out with the support of the Ministry of Science and Higher Education of the Russian Federation within the framework of a state assignment (project No. FZGM-2023-0006). V.A. Makagonov reports financial support was provided by The work was carried out with the support of the Ministry of Science and Higher Education of the Russian Federation within the framework of a state assignment (project No. FZGM-2023-0006). V.A.

Foshin reports financial support was provided by The work was carried out with the support of the Ministry of Science and Higher Education of the Russian Federation within the framework of a state assignment (project No. FZGM-2023-0006). Y.E. Kalinin reports a relationship with Voronezh State Technical University, 394006 Voronezh, Russia that includes: employment. A.V. Sitnikov reports a relationship with Voronezh State Technical University, 394006 Voronezh, Russia that includes: employment. V.A. Makagonov reports a relationship with Voronezh State Technical University, 394006 Voronezh, Russia that includes: employment. V.A. Foshin reports a relationship with Voronezh State Technical University, 394006 Voronezh, Russia that includes: employment. M.N. Volochaev reports a relationship with Kirensky Institute of Physics, 660036 Krasnoyarsk, Russia that includes: employment. I.M. Pripechenkov reports a relationship with Faculty of Physics, Lomonosov Moscow State University, 119991 Moscow, Russia that includes: employment. N.N. Perova reports a relationship with Faculty of Physics, Lomonosov Moscow State University, 119991 Moscow, Russia that includes: employment. E.A. Ganshina reports a relationship with Faculty of Physics, Lomonosov Moscow State University, 119991 Moscow, Russia that includes: employment. V.V. Rylkov reports a relationship with National Research Center Kurchatov Institute, 123182 Moscow, Russia that includes: employment. A.B. Granovsky reports a relationship with Faculty of Physics, Lomonosov Moscow State University, 119991 Moscow, Russia that includes: employment. If there are other authors, they declare that they have no known competing financial interests or personal relationships that could have appeared to influence the work reported in this paper.

Data availability

Data will be made available on request.

Acknowledgments

The work was carried out with the support of the Ministry of Science and Higher Education of the Russian Federation within the framework of a state assignment (project No. FZGM-2023-0006)

References

- [1] D.E. Burgler, M. Buchmeier, S. Cramm, S. Eisebitt, R.R. Gareev, P. Grunberg, C. L. Jia, L.L. Pohlmann, R. Schreiber, M. Siegel, Y.L. Qin, A. Zimina, Exchange coupling of ferromagnetic films across metallic and semi-conducting interlayers, *J. Phys. Condens. Matter* 15 (2003) 443–450, <https://doi.org/10.1088/0953-8984/15/5/301>.
- [2] Y. Guo, X.W. Yu, Y.X. Li, Spin filtering and spin-polarization reversal in multilayered ferromagnetic metal/semiconductor heterostructures, *J. Appl. Phys.* 98 (5) (2005) 053902–053907, <https://doi.org/10.1063/1.2030410>.
- [3] W. Amamou, I.V. Pinchuk, A.H. Trout, R. Williams, N. Antolin, A. Goad, D. J. O'Hara, A.S. Ahmed, W. Windl, D.W. McComb, R.K. Kawakami, Magnetic proximity effect in Pt/CoFe₂O₄ bilayers, *Phys. Rev. Materials* 2 (2018) 011401(R), <https://doi.org/10.1103/PhysRevMaterials.2.011401>.
- [4] D. Zhong, K.L. Seyler, X. Linpeng, N.P. Wilson, T. Taniguchi, K. Watanabe, M. A. McGuire, K.M.C. Fu, D. Xiao, W. Yao, X. Xu, Layer-resolved magnetic proximity effect in van der Waals heterostructures, *Nat. Nanotechnol.* 15 (2020) 187–191, <https://doi.org/10.1038/s41565-019-0629-1>.
- [5] J. Hu, J. Luo, Y. Zheng, J. Chen, G.J. Omar, A.T.S. Wee, A. Ariando, Magnetic proximity effect at the interface of two-dimensional materials and magnetic oxide insulators, *J. Alloy. Compd.* 911 (2022) 164830, <https://doi.org/10.1016/j.jallcom.2022.164830>.
- [6] E.A. Yadkina, A.A. Vorobiev, V.A. Ukleev, D. Lott, A.V. Sitnikov, Y.E. Kalinin, O. V. Gerashchenko, S.V. Grigoriev, Morphology and the magnetic and conducting properties of heterogeneous layered magnetic structures $[(\text{Co}_{45}\text{Fe}_{45}\text{Zr}_{10})_{35}(\text{Al}_2\text{O}_3)_{65}/\text{a-Si:H}]_{36}$, *J. Exp. Theor. Phys.* 118 (3) (2014) 410–416, <https://doi.org/10.1134/S1063776114020083>.
- [7] S.V. Komogortsev, E.A. Denisova, R.S. Iskhakov, A.D. Balaev, L.A. Chekanova, Y. E. Kalinin, A.V. Sitnikov, Multilayer nanogranular films $(\text{Co}_{40}\text{Fe}_{40}\text{B}_{20})_{50}(\text{SiO}_2)_{50}/\text{a-Si:H}$ and $(\text{Co}_{40}\text{Fe}_{40}\text{B}_{20})_{50}(\text{SiO}_2)_{50}/\text{SiO}_2$: magnetic properties, *J. Appl. Phys.* 113 (17) (2013) 17C105, <https://doi.org/10.1063/1.4794361>.
- [8] E.A. Ganshina, N.S. Perov, S. Phonghirun, V.E. Migunov, Y.E. Kalinin, A. V. Sitnikov, Enhancement of magneto-optical response in nanocomposite-hydrogenated amorphous silicon multilayers, *Bull. Russ. Acad. Sci. Phys.* 72 (10) (2008) 1379–1381, <https://doi.org/10.3103/S1062873808100201>.

- [9] O.V. Dunets, Y.E. Kalinin, M.A. Kashirin, A.V. Sitnikov, Electrical and magnetic performance of multilayer structures based on $(\text{Co}_{40}\text{Fe}_{40}\text{B}_{20})_{33.9}(\text{SiO}_2)_{66.1}$ composite, *Tech. Phys.* 58 (9) (2013) 1352–1357, <https://doi.org/10.1134/S1063784213090132>.
- [10] B.B. Straumal, A.A. Mazilkin, S.G. Protasova, A.A. Myatiev, P.B. Straumal, G. Schütz, P.A. van Aken, E. Goering, B. Baretzky, Magnetization study of nanograined pure and Mn-doped ZnO films: formation of a ferromagnetic grain-boundary foam, *Phys. Rev. B: Condensed Matter* 79 (20) (2009) 205206, <https://doi.org/10.1103/PhysRevB.79.205206>.
- [11] A.S. Kuz'mina, A.A. Lotin, O.A. Novodvorsky, N.S. Perov, E.A. Gan'shina, L. A. Makarova, A.S. Semisalova, A.G. Shneider, M.P. Kuz'min, S.S. Kolesnikov, Magnetism and magneto-optics features of $\text{Zn}_{1-x}\text{Co}_x\text{O}_y$ thin films grown by pulsed laser deposition, *Mater. Chem. Phys.* 198 (2017) 291–296, <https://doi.org/10.1016/j.matchemphys.2017.06.015>.
- [12] J. Wu, M. Gong, ZnO/graphene heterostructure nanohybrids for optoelectronics and sensors, *J. Appl. Phys.* 130 (7) (2021) 070905, <https://doi.org/10.1063/5.0060255>.
- [13] Ü. Özgür, Ya.I. Alivov, C. Liu, A. Teke, M.A. Reshchikov, S. Doğan, V. Avrutin, S.-J. Cho, H. Morkoç, A comprehensive review of ZnO materials and devices, *J. Appl. Phys.* 98(4) (2005), 041301-041301-103, doi: 10.1063/1.1992666.
- [14] M.N. Martyshev, A.V. Emelyanov, V.A. Demin, K.E. Nikiruy, A.A. Minnekhanov, S. N. Nikolaev, A.N. Taldenkov, A.V. Ovcharov, M.Y. Presnyakov, A.V. Sitnikov, A. L. Vasiliev, P.A. Forsh, A.B. Granovsky, P.K. Kashkarov, M.V. Kovalchuk, V. V. Rylkov, Multifilamentary character of anticorrelated capacitive and resistive switching in memristive structures based on $(\text{Co}-\text{Fe}-\text{B})_x(\text{LiNbO}_3)_{100-x}$ nanocomposite, *Phys. Rev. Appl.* 14 (3) (2020) 034016, <https://doi.org/10.1103/PhysRevApplied.14.034016>.
- [15] V.V. Rylkov, S.N. Nikolaev, K.Y. Chernoglazov, V.A. Demin, A.V. Sitnikov, M. Y. Presnyakov, A.L. Vasiliev, N.S. Perov, A.S. Vedenev, Y.E. Kalinin, V. V. Tugushev, A.B. Granovsky, Tunneling anomalous Hall effect in nanogranular CoFe-B-Al-O films near the metal-insulator transition, *Phys. Rev. B* 95 (2017) 144402, <https://doi.org/10.1103/PhysRevB.95.144202>.
- [16] V.V. Rylkov, V.A. Demin, A.V. Emelyanov, A.V. Sitnikov, Y.E. Kalinin, V. V. Tugushev, A.B. Granovsky, Magnetic metal-nonstoichiometric oxide nanocomposites: structure, transport and memristive properties, in: V. Domracheva, M. Capoli, E. Rentschler (Eds.), *Novel Magnetic Nanostructures: Unique Properties and Applications*, Elsevier, Amsterdam, 2018, pp. 426–463, <https://doi.org/10.1016/B978-0-12-813594-5.00013-8>.
- [17] E.A. Gan'shina, A.B. Granovsky, V.V. Garshin, I.M. Pripechenkov, A.V. Sitnikov, M. N. Volochaev, V.V. Ryl'kov, S.N. Nikolaev, Magneto-optical spectroscopy of nanocomposites $(\text{CoFeZr})_x(\text{Al}_2\text{O}_3)_{100-x}$, *SPIN* 13 (2023) 2340006, <https://doi.org/10.1142/S2010324723400064>.
- [18] E.A. Gan'shina, V.V. Garshin, N.N. Perova, I.M. Pripechenkov, A.N. Yurasov, M. M. Yashin, V.V. Rylkov, A.B. Granovskii, Magneto-optical Kerr spectroscopy of nanocomposites, *J. Exp. Theor. Phys.* 137 (2023) 572–581, <https://doi.org/10.1134/S1063776123100151>.
- [19] A. Ashour, M.A. Kaid, N.Z. El-Sayed, A.A. Ibrahim, Physical properties of ZnO thin films deposited by spray pyrolysis technique, *Appl. Surf. Sci.* 252 (22) (2006) 7844–7848, <https://doi.org/10.1016/j.apsusc.2005.09.048>.
- [20] S.A. Gridnev, Y.E. Kalinin, A.V. Sitnikov, O.V. Stognei, *Nonlinear Phenomena in Nano- and Microheterogeneous Systems*, BINOM, Lab knowledge Publ, Moscow, 2012 (in Russian).
- [21] B.B. Straumal, S.G. Protasova, A.A. Mazilkin, G. Schütz, E. Goering, B. Baretzky, P. B. Straumal, Ferromagnetism of zinc oxide nanograined films, *JETP Lett.* 97 (2013) 367–377, <https://doi.org/10.1134/S0021364013060143>.
- [22] X. Wu, Z. Wei, L. Zhang, X. Wang, H. Yang, J. Jiang, Optical and magnetic properties of Fe doped ZnO nanoparticles obtained by hydrothermal synthesis, *J. Nanomater.* 792102 (2014), <https://doi.org/10.1155/2014/792102>.
- [23] V.V. Rylkov, A.V. Emelyanov, S. Nikolaev, K.E. Nikiruy, A.V. Sitnikov, E. Fadeev, V.A. Demin, A.B. Granovsky, Transport properties of magnetic nanogranular composites with dispersed ions in an insulating matrix, *J. Exp. Theor. Phys.* 131 (1) (2020) 160–176, <https://doi.org/10.1134/S1063776120070109>.
- [24] J.M.D. Coey, A.P. Douvalis, C.B. Fitzgeld, M. Venkatsen, Ferromagnetism in Fe-doped SnO_2 thin films, *Appl. Phys. Lett.* 84 (3) (2004) 1332–1334, <https://doi.org/10.1063/1.1650041>.
- [25] S. Bedanta, T. Eimüller, W. Kleemann, J. Rhensius, F. Stromberg, E. Amaladass, S. Cardoso, P. Freitas, Overcoming the dipole disorder in dense CoFe nanoparticle ensembles: superferromagnetism, *Phys. Rev. Lett.* 98 (2007) 176601, <https://doi.org/10.1103/PhysRevLett.98.176601>.
- [26] S. Bedanta, W. Kleemann, Supermagnetism, *J. Phys. D: Applied Physics* 42 (1) (2008) 013001, <https://doi.org/10.1088/0022-3727/42/1/013001>.
- [27] E.A. Gan'shina, A.B. Granovsky, A.V. Sitnikov, E. Lahderanta, V.V. Rylkov, Magneto-optical spectroscopy of $(\text{CoFeB})_x(\text{Al}-\text{O})_{100-x}$ nanocomposites: evidence of superferromagnetism, *IEEE Magn. Lett.* 11 (2020) 1–4, <https://doi.org/10.1109/lmag.2019.2963874>.
- [28] E. Kulatov, O. Novodvorski, V. Rylkov, E. Gan'shina, D. Shevyakov, V. Tugushev, Y. Uspenskii, Electronic and magneto-optical properties of ZnO:Co, *EPJ Web Conf.* 185 (2018) 06012, <https://doi.org/10.1051/epjconf/201818506012>.
- [29] M.I. Blinov, M.A. Shakhov, V.V. Rylkov, E. Lahderanta, V.N. Prudnikov, S. N. Nikolaev, A.V. Sitnikov, A.B. Granovsky, Magnetoresistance of $(\text{Co}_{40}\text{Fe}_{40}\text{B}_{20})_x(\text{SiO}_2)_{100-x}$ and $(\text{Co}_{84}\text{Nb}_{14}\text{Ta}_2)_x(\text{Al}_2\text{O}_3)_{100-x}$ nanocomposites below the percolation threshold in pulsed magnetic fields, *J. Magn. Magn. Mater.* 469 (2019) 155–160, <https://doi.org/10.1016/j.jmmm.2018.08.023>.
- [30] E.A. Fadeev, E. Lahderanta, B.A. Aronzon, A.B. Mekhiya, Yu.E. Kalinin, V. A. Makagonov, S.Yu Pankov, V.A. Foshin, A.B. Granovsky, Unconventional magnetoresistance in ZnO/C multilayers at low temperatures, *J. Magn. Magn. Mater.* 535 (2021), <https://doi.org/10.1016/j.jmmm.2021.167963>.
- [31] J. Inoue, S. Maekawa, Theory of tunneling magnetoresistance in granular magnetic films, *Phys. Rev. B* 53 (18) (1996) R11927–R11929, <https://doi.org/10.1103/PhysRevB.53.R11927>.
- [32] P. Sheng, B. Abeles, Y. Arie, Hopping conductivity in granular metals, *Phys. Rev. Lett.* 31 (1973) 44, <https://doi.org/10.1103/PhysRevLett.31.44>.
- [33] J.C. Slonczewski, Conductance and exchange coupling of two ferromagnets separated by a tunneling barrier, *Phys. Rev. B* 39 (10) (1989) 6995–7002, <https://doi.org/10.1103/PhysRevB.39.6995>.
- [34] S.N. Nikolaev, K.Yu Chernoglazov, A.V. Emelyanov, A.V. Sitnikov, A.N. Taldenkov, T.D. Patsaev, A.L. Vasiliev, E.A. Gan'shina, V.A. Demin, N.S. Averkiev, A. B. Granovsky, V.V. Rylkov, $(\text{CoFeB})_x(\text{LiNbO}_3)_{100-x}/\text{Si}$ Nanocomposite film structures below the percolation threshold: manifestations of the cotunneling and exchange effects, *JETP Lett.* 118 (1) (2023) 58–66, <https://doi.org/10.1134/S0021364023601550>.
- [35] I.S. Beloborodov, A.V. Lopatin, V.M. Vinokur, K.B. Efetov, Granular electronic systems, *Rev. Mod. Phys.* 79 (2) (2007) 469, <https://doi.org/10.1103/RevModPhys.79.469>.
- [36] M.V. Feigel'man, A.S. Ioselevich, Variable range cotunneling and conductivity of a granular metal, *JETP Lett.* 81 (6) (2005) 277–283, <https://doi.org/10.1134/1.1931015>.